The First GECAM Observation Results on Terrestrial Gamma-ray Flashes and Terrestrial Electron Beams

Y. Zhao[1,2], J. C. Liu[2,3], S. L. Xiong[2], W. C. Xue[2,3], Q. B. Yi[4,2], G. P. Lu[5], W. Xu[6], F. C. Lyu[7], J. C. Sun[2], W. X. Peng[2], C. Zheng[2,3], Y. Q. Zhang[2,3], C. Cai[8], S. Xiao[9,10], S. L. Xie[11], C. W. Wang[2,3], W. J. Tan[2,3], Z. H. An[2], G. Chen[2], Y. Q. Du[12,2], Y. Huang[2], M. Gao[2], K. Gong[2], D. Y. Guo[2], J. J. He[2], B. Li[2], G. Li[2], X. Q. Li[2], X. B. Li[2], J. Liang[12,2], X. H. Liang[2], Y. Q. Liu[2], X. Ma[2], R. Qiao[2], L. M. Song[2], X. Y. Song[2], X. L. Sun[2], J. Wang[2], J. Z. Wang[2], P. Wang[2], X. Y. Wen[2], H. Wu[12,2], Y. B. Xu[2], S. Yang[2], B. X. Zhang[2], D. L. Zhang[2], F. Zhang[2], P. Zhang[13,2], H. M. Zhang[2], Z. Zhang[2], X. Y. Zhao[2], S. J. Zheng[2], K. K. Zhang[14], X. B. Han[14], H. Y. Wu[15], T. Hu[15], H. Geng[15], F. J. Lu[2], S. N. Zhang[2], H. Yu[1]

[1]Department of Astronomy, Beijing Normal University, Beijing 100875, Beijing, China
[2]Key Laboratory of Particle Astrophysics, Institute of High Energy Physics, Chinese Academy of Sciences, Beijing 100049, Beijing, China
[3]University of Chinese Academy of Sciences, Beijing 100049, Beijing, China
[4]School of Physics and Optoelectronics, Xiangtan University, Xiangtan 411105, Hunan, China
[5]School of Earth and Space Sciences, University of Science and Technology of China, Hefei 230026, Anhui, China
[6]Electronic Information School, Wuhan University, Wuhan 430072, Hubei, China
[7]Key Laboratory of Transportation Meteorology of China Meteorological Administration, Nanjing Joint Institute for Atmospheric Sciences, Nanjing 210000, Jiangsu China
[8]College of Physics and Hebei Key Laboratory of Photophysics Research and Application, Hebei Normal University, Shijiazhuang, Hebei 050024, China
[9]Guizhou Provincial Key Laboratory of Radio Astronomy and Data Processing, Guizhou Normal University, Guiyang 550001, GuiZhou, China
[10]School of Physics and Electronic Science, Guizhou Normal University, Guiyang 550001, GuiZhou, China
[11]Institute of Astrophysics, Central China Normal University, Wuhan 430079, HuBei, China
[12]School of Computing and Artificial Intelligence, Southwest Jiaotong University, Chengdu 611756, SiChuan, China
[13]College of Electronic and Information Engineering, Tongji University, Shanghai 201804, Shanghai, China
[14]Innovation Academy for Microsatellites of Chinese Academy of Sciences, Shanghai 201304, Shanghai, China
[15]National Space Science Center, Chinese Academy of Sciences, Beijing 100190, Beijing, China

Key Points:

- GECAM can well classify and distinguish TGF/TEB, and reveal their fine temporal and spectral features, e.g. short spikes down to 10 ms.
- GECAM discovered an interesting two-peaked TEB which is probably from a lightning process near the geomagnetic footprint.
- TGF-lightning association rate between GECAM and GLD360 in east Asia is found to be $\sim 80\%$, notably higher than previous reports.

Corresponding author: S. L. Xiong, `xiongsl@ihep.ac.cn`

Abstract

Gravitational wave high-energy Electromagnetic Counterpart All-sky Monitor (GECAM) is a space-borne instrument dedicated to monitoring high-energy transients, thereinto Terrestrial Gamma-ray Flashes (TGFs) and Terrestrial Electron Beams (TEBs). We propose a TGF/TEB search algorithm, with which 147 bright TGFs and 4 TEBs are identified during an effective observation time of $\sim$ 9 months. We show that, with gamma-ray and charged particle detectors, GECAM can effectively identify and distinguish TGFs and TEBs, and measure their temporal and spectral properties in detail. Moreover, we find an interesting TEB consisting of two pulses with a separation of $\sim$ 150 ms, which is expected to originate from a lightning process near the geomagnetic footprint. We also find that the GECAM TGF's lightning-association ratio is $\sim$ 80% in the east Asia region using the GLD360 lightning network, which is significantly higher than previous observations.

Plain Language Summary

Terrestrial gamma-ray flashes (TGFs) and Terrestrial Electron Beams (TEBs) are one of the most energetic radioactive phenomena in the atmosphere of the Earth. They reflect a natural particle accelerator that can boost electrons up to at least several tens of mega electron volts (MeV). With novel detection technologies, GECAM is a new powerful instrument to observe TGFs and TEBs, as well as study their properties. For example, it is difficult for most space-borne high-energy instruments to distinguish between TGFs and TEBs. With the joint observation of gamma-ray and charged particle detectors, GECAM can effectively identify TGFs and TEBs. GECAM can also reveal fine features in the light curves and spectra of these bursts. Interestingly, GECAM discovered the first, as far as we are aware of, TEB which consists of two pulses with a separation time of about 150 ms. Unlike the case in previous TEBs, the second pulse is not the return peak but has the same origin as the first one.

1 Introduction

Terrestrial Gamma-ray Flashes (TGFs) are submillisecond intense bursts of γ-rays with energies up to several tens of MeV (Briggs et al., 2010; Marisaldi et al., 2010, 2019), which was serendipitously discovered by the Burst and Transient Source Experiment (BATSE) aboard Compton Gamma-ray Observatory (CGRO) in 1991 (Fishman et al., 1994). Since then, TGFs have been routinely observed by space-borne instruments, such as BeppoSAX (Ursi et al., 2017), RHESSI (Grefenstette et al., 2009), AGILE (Marisaldi et al., 2010), *Fermi*/GBM (Roberts et al., 2018) and ASIM (Østgaard et al., 2019) during last three decades. Occasionally, TGFs can also be observed by ground instruments (Dwyer et al., 2012), however, the strong absorption of gamma-rays in the air makes the detection very difficult.

TGFs observed by these space-borne instruments are widely believed to be produced through the initial upward leader of positive Intracloud (+IC) lightning (Lu et al., 2010, 2011). They are the results of relativistic electrons that produce hard X/γ-rays through the bremsstrahlung process. These electrons are accelerated in a very high electric field by the runaway process (Wilson, 1925) and multiplied by many orders of magnitude through the Relativistic Runaway Electron Avalanche process (Gurevich et al., 1992; Dwyer & Smith, 2005). Two main models were proposed to explain the production of TGFs. One is the lightning leader model, which involves the acceleration of free electrons under the localized electric field in front of lightning leader tips (Moss et al., 2006; Dwyer, 2010; Celestin & Pasko, 2011; Celestin et al., 2013). The other one is the relativistic feedback model (RFD) (Dwyer, 2003; Dwyer, 2008, 2012; Liu & Dwyer, 2013), which considers the feedback processes from positrons and photons in a large-scale electric field region.

However, the specific mechanism to produce $\sim 10^{17}$ to 10^{19} electrons is still an open question (Chanrion & Neubert, 2010; Xu et al., 2012, 2015; Skeltved et al., 2017).

By interacting with the atmosphere during the propagation, the TGF photons can produce secondary electrons and positrons. Then they will move along the Earth's magnetic field line, forming Terrestrial Electron Beams (TEBs) (Dwyer et al., 2008), which could be observed by some TGF-detecting instruments (Xiong et al., 2012; Lindanger et al., 2020; Sarria et al., 2021).

In this study, the data of Gravitational-wave high-energy Electromagnetic Counterpart All-sky Monitor (GECAM) (Li et al., 2022) are utilized for TGFs and TEBs research. GECAM is a space-based instrument dedicated to the observation of gamma-ray electromagnetic counterparts of the Gravitational Waves (Goldstein et al., 2017) and Fast Radio Bursts (Lorimer et al., 2007), as well as other high-energy astrophysical and terrestrial transient sources, such as Gamma-ray Bursts (GRBs) (Klebesadel et al., 1973), Soft Gamma-ray Repeaters (SGRs) (Woods & Thompson, 2004), solar flares, TGFs and TEBs.

2 Instrument and Search Algorithm

Since the launch in December 2020, GECAM has been operating in low earth orbit (600 km altitude and 29° inclination angle) (Han et al., 2020). GECAM consists of twin micro-satellites (i.e. GECAM-A and GECAM-B) and each of them comprises 25 Gamma-ray Detectors (GRDs) (An et al., 2022) and 8 Charged Particle Detectors (CPDs) (Xu et al., 2022). It should be noted that only GECAM-B data are utilized in this study because GECAM-A has not been able to observe yet (Li et al., 2022).

With $LaBr_3$ crystals read out by silicon photomultiplier (SiPM) arrays, GRDs can detect high-energy photons in a broad energy range of $\sim$ 15 keV to $\sim$ 5 MeV (Zhang et al., 2022). CPDs are designed to detect the charged particles from $\sim$ 100 keV to $\sim$ 5 MeV. The joint observation of GRDs and CPDs can distinguish between gamma-rays and charged particle bursts, such as TGFs and TEBs (Zhao et al., 2021).

To detect those extremely short and bright bursts, e.g. TGFs and TEBs, a dedicated anti-saturation data acquisition system (DAQ) is designed for GECAM. The data buffer in DAQ can accommodate up to 4092 and 1020 counts for the high-gain and low-gain of each GRD, respectively. Since there are usually several hundred counts registered for a bright TGF, the GECAM DAQ can guarantee to transfer and save almost all TGFs photons that are recorded by detectors (Liu et al., 2021).

For GRD, the dead time is 4 μs for normal events and $>$ 69 μs for overflow events (i.e. events with higher energy deposition than the maximum measurable energy). Each GRD detector has two read-out channels: high-gain channel ($\sim$ 15 keV to $\sim$ 300 keV) and low-gain channel ($\sim$ 300 keV to $\sim$ 5 MeV) (Liu et al., 2021). The design, performance, and other information about GECAM have been reported by Li et al. (2022); An et al. (2022); Xu et al. (2022).

The considerable number of GRD detectors is helpful to locate the source region of TGFs. We have proposed a dedicated localization method for all-sky monitor which can be used for extremely short-duration TGFs (Zhao et al. 2022a). Despite the low counting statistics of TGFs, GECAM can still locate TGFs (Zhao et al. 2022b).

As the main contamination source for TGFs, cosmic-ray events show very similar patterns in data as TGFs, but with an even shorter duration. Thanks to the high time resolution of GECAM, i.e. 100 ns (Xiao et al., 2022), GECAM can effectively distinguish between cosmic-ray events and TGFs. Indeed, a dedicated data product called Simultaneous Events is designed for GECAM. The Simultaneous Events Number (SimEvtNum) is defined as the number of events from different detectors registered in the same 300 ns time window (Xiao et al., 2022). As the SimEvtNum increases, the probability of these events caused by cosmic-rays surges. Here a relatively loose criterion (SimEvtNum $>$ 13) is adopted for basic data selection.

To unveil TGFs and TEBs in GECAM data, we developed a dedicated burst search algorithm, which is very different from normal burst search for gamma-ray bursts (Cai et al., 2021, 2022), because the TGF and TEB are so weak that only a few counts are registered in each detector, and both GRDs and CPDs are needed in the search. The event-by-event (EVT) data of GECAM GRDs and CPDs are used in this study. Only recommended normal events with SimEvtNum $<$ 13 are utilized. We divide 25 GRDs into four groups considering the neighboring position, and it turns out that there are 6 [7] GRDs for 3 [1] group(s). All 8 CPDs are treated as a single group.

Assuming the background follows the Poisson distribution, the probability that the counts are from background fluctuation can be calculated as,

$$P_{\rm group}(S \geq S^{'}|B) = 1 - \sum_{S=0}^{S=S^{'}-1} \frac{B^S \cdot \exp(-B)}{S!}, \quad (1)$$

where S and $S^{'}$ are observed counts and threshold counts, respectively, for one group in a time window, B is the estimated background for the time window calculated by the average counts over $T_{\rm rela} \in$ [-5,-1] s and $\in$ [+1,+5] s, where $T_{\rm rela}$ is the relative time with respect to the end time of the time window.

For an individual searching bin, the joint probability of at least $N^{'}_{\rm trig}$ group(s) out of total group number M passing the trigger threshold for a single group $P_{\rm group}$ is,

$$P_{\rm bin}(N_{\rm trig} \geq N^{'}_{\rm trig}) = \sum_{N_{\rm trig}=N^{'}_{\rm trig}}^{N_{\rm trig}=M} C_M^{N_{\rm trig}} \cdot (P_{\rm group})^{N_{\rm trig}} \cdot (1-P_{\rm group})^{M-N_{\rm trig}}. \quad (2)$$

In this work, seven time scales are utilized to do searching. The widths of time scales with the corresponding empirical threshold $P_{\rm tot}$ are: 50 μs (5.0×10^{-22}), 100 μs (2.0×10^{-21}), 250 μs (1.3×10^{-20}), 500 μs (5.0×10^{-20}), 1 ms (2.0×10^{-19}), 2 ms (8.0×10^{-19}), 4 ms (3.2×10^{-18}). All of them are used for TGF search while only the latter four are for TEB search. It should be noted that these empirical criteria are relatively strict so that only intense TGFs or TEBs could be identified.

By setting $P_{\rm tot} = P_{\rm bin}$, the group's trigger threshold ($P_{\rm group,GRD}$) can be obtained for TGF with GRDs from the following equation (i.e. $M = 4$, and we set $N^{'}_{\rm trig,GRD} = 2$),

$$P_{\rm tot,GRD}(N_{\rm trig} \geq 2) = 6 \cdot P^2_{\rm group,GRD} - 8 \cdot P^3_{\rm group,GRD} + 3 \cdot P^4_{\rm group,GRD}, \quad (3)$$

and the trigger threshold from the following equation of TEB with CPDs ($M = 1$, and we set $N^{'}_{\rm trig,CPD} = 1$),

$$P_{\rm tot,CPD} = P_{\rm group,CPD}. \quad (4)$$

According to the empirical threshold above, the trigger threshold for each detector group can be obtained for each searching window, e.g. for 100 μs, $P_{\rm group,GRD} = 1.8 \times 10^{-11}$ which corresponds to 6.6 σ in standard Gaussian distribution.

For a candidate to be identified as a TGF/TEB, all criteria below must be met:

1. The trigger threshold (Equations 3 and 4) must be satisfied.
2. The candidate should not be SGR. It should be noticed that millisecond-duration SGRs can be searched in the time scale of milliseconds with a much softer spectrum than TGFs.
3. Should not be caused by instrument effects, which are characterized by that there is significant excess (Poisson significance $> 6\ \sigma$) registered in 2 to 3 GRDs while no obvious signals (Poisson significance $< 3\ \sigma$) for most (i.e. > 21) GRDs.
4. For filtering out cosmic-rays, the ratio of the simultaneous event ($R_{\rm sim,7}$[1]) should be $< 20\%$.

[1] $R_{\rm sim,7}$: the total number of simultaneous events registered in > 7 GRDs, divided by the total events number in the searching bin.

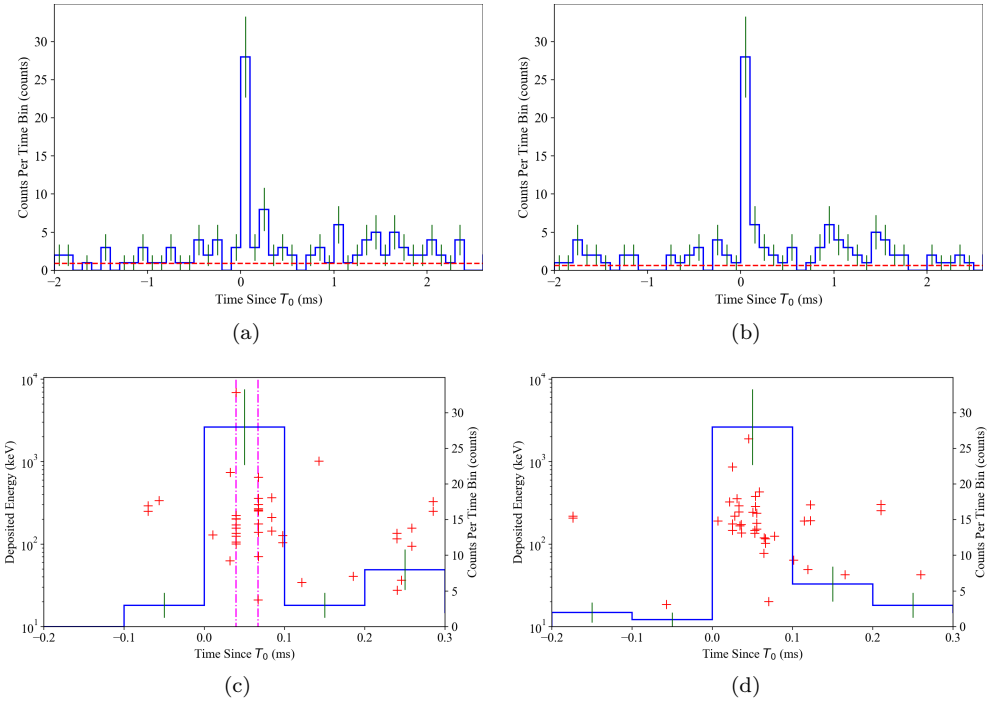

Figure 1. Illustration of distinguishing between cosmic-rays and TGFs by simultaneous events. (a) and (c): the light curve and time-energy scatter plot of a cosmic-ray event. (b) and (d): the light curve and time-energy scatter plot of a TGF. The dot-dashed lines show the time edge of simultaneous events registered in > 7 GRDs within 300 ns. The horizontal and vertical scales are the same for the two events.

For the identification of TEBs, more criteria are needed which will be described in Section 4. To further illustrate the capability of GECAM to identify cosmic-rays, a case is illustrated in Figure 1. The classification of the two excesses can not be distinguished well just according to the light curves. However, the cosmic-ray event (Figure 1a and 1c has $F_{\mathrm{sim},7} = \frac{18}{28} \approx 64\%$, while TGFs have no simultaneous events registered in > 7 GRDs (Figure 1b and 1d).

3 GECAM TGFs

From December 10th, 2020 to August 31st, 2022, the effective observation time of GECAM-B is $\sim$ 274.5 days ($\sim$ 0.75 years). As shown in Figure 2, 147 bright TGFs are identified by our search algorithm, corresponding to a discovery rate of $\sim$ 200 TGFs/year or 0.54 TGFs/day. The Global Lightning Dataset (GLD360) is utilized to match lightning for GECAM TGFs in the time window of $\pm$ 5 ms corrected for the light propagation time and within the distance window of 800 km from GECAM nadirs. The GLD360 lightning-association ratio is $\frac{34}{42} \approx 80\%$ in the east Asia region (EAR, 77° E–138° E, 13° S–30° N) which is $\sim$ 2.5 times of the results based on the data of the other spaceborne instruments and the World Wide Lightning Location Network (WWLLN) lightning ($\sim$ 33%) (Roberts et al., 2018; Maiorana et al., 2020). The high lightning-association ratio may be attributed to two factors: (1) the detection efficiency of GLD360 is higher than the other lightning location network at least in EAR (Said et al., 2013; Poelman et al., 2013; Pohjola & Mäkelä, 2013), (2) the current GECAM TGF sample only contains bright ones, resulting from the very strict searching threshold. The sphere distance between the GECAM nadirs and the associated GLD360 lightning inside the EAR ranges from $\sim$ 50 km to 800 km, which is consistent with previous reports.

The statistical distribution of temporal, intensity and energy properties of this GECAM TGF sample are shown in Figure 3. The duration is calculated by the Bayesian Block (BB) algorithm (Scargle et al., 2013). Since the relatively strict threshold, faint TGFs are dropped from the current sample. Therefore, the GECAM TGF discovery rate would increase as we decrease the search threshold in the future. As shown in Figure 3c, TGF events with relatively shorter duration tend to have a harder spectrum and thus more high-energy electrons in the source region, which is in line with previous observations (Briggs et al., 2013). As shown in Figure 3d, the duration and CPD/GRD counts ratio is very effective to classify TGFs and TEBs (see Section 4).

In Figure 4, the light curves and time-energy scatter plots are illustrated for three multipeak, three bright, and two short TGFs. The fraction of multipeak TGFs is $\frac{3}{147} \approx 2\%$, which is consistent with that observed by the other instruments (Mezentsev et al., 2016; Lindanger et al., 2020). Since the upward leader channel of a lightning discharge would generally branch into several channels during propagation, it is widely accepted that the temporal structures may reflect the electric field distribution that the leaders have passed through. This effect is more pronounced in the multipeak or overlapping structures of TGFs.

It is worth noticing an interesting double-peaked TGF (Figure 4a) which is characterized by two $\sim$ 100 μs pulses with very similar temporal and spectral structures. Two possible scenarios may explain this double-peaked TGF. For the first, it could be associated with two leader branches propagating in two distinct localized electric fields, which could be also responsible for the cases shown in Figure 4b to 4c. However, this double-peak TGF (Figure 4a) may require coincidences comparing to other TGFs in Figure 4b to 4c, i.e. two intracloud electric fields with similar distribution on the passageway of these upward leader channels. For the second, it could be associated with two successive steps of one propagating channel. We note that the time interval between the two pulses of this double-peak TGF is generally consistent with the typical duration of the stepped leader's step, i.e., $\sim$ 0.1 ms (Lyu et al., 2016). Meanwhile, the typical length of leader steps during intracloud lightning discharge is from several hundred meters to several kilometers (Stolzenburg et al., 2016). Therefore, the second pulse of this TGF was also likely generated after the initial leader (which resulted in the first pulse) propagated forward for one or several more steps.

We also find that the overlapping pulse of a TGF could be as short as $\sim$ 10 μs (Figure 4f). These fine structures in light curves provide new insights into the specific electric field distribution of lightning discharge. Since the tails of TGFs are usually soft (Nemiroff

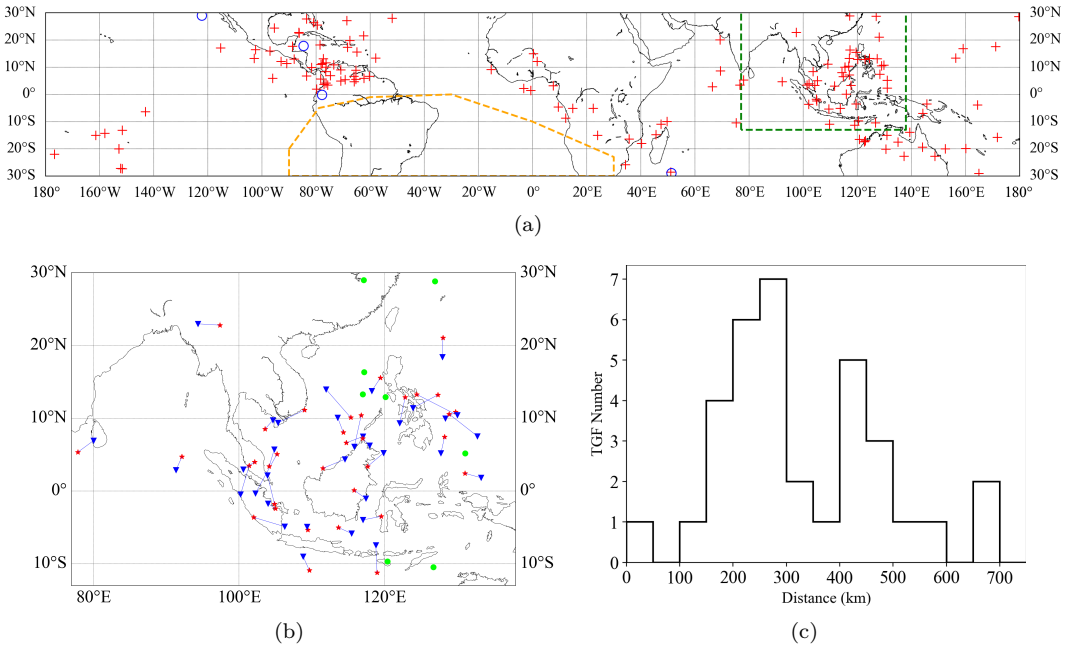

Figure 2. Geographical distribution of GECAM TGFs. (a) GECAM nadirs of 147 TGFs (fuchsia pluses) and 4 TEBs (blue circles). The green and orange dashed lines show the east Asia region (EAR, 77° E–138° E, 13° S–30° N) and South Atlantic Anomaly (SAA), respectively. (b) The red[lime] markers illustrate the TGFs with[without] associated GLD360 lightning inside the EAR. The blue triangles illustrate the associated lightning within ± 5 ms corrected for the light travel time and within 800 km from GECAM nadirs. (c) The distribution of sphere distance between the GECAM nadirs and their associated GLD360 lightning inside the EAR.

et al., 1997; Feng et al., 2002), the high-gain channels of GRDs (down to ∼15 keV) are suitable to detect these tails (see Figure 4d to 4f). Furthermore, thanks to the high time resolution and a large number of GRD detectors provided by GECAM, some short-duration (down to 37 μs) TGFs are found, as shown in Figure 4g to 4h. There are more than 40 counts registered in such a short duration of 37 μs, indicating an extremely high counts rate of $\sim$ 1.1 million counts/s (see Figure 4g).

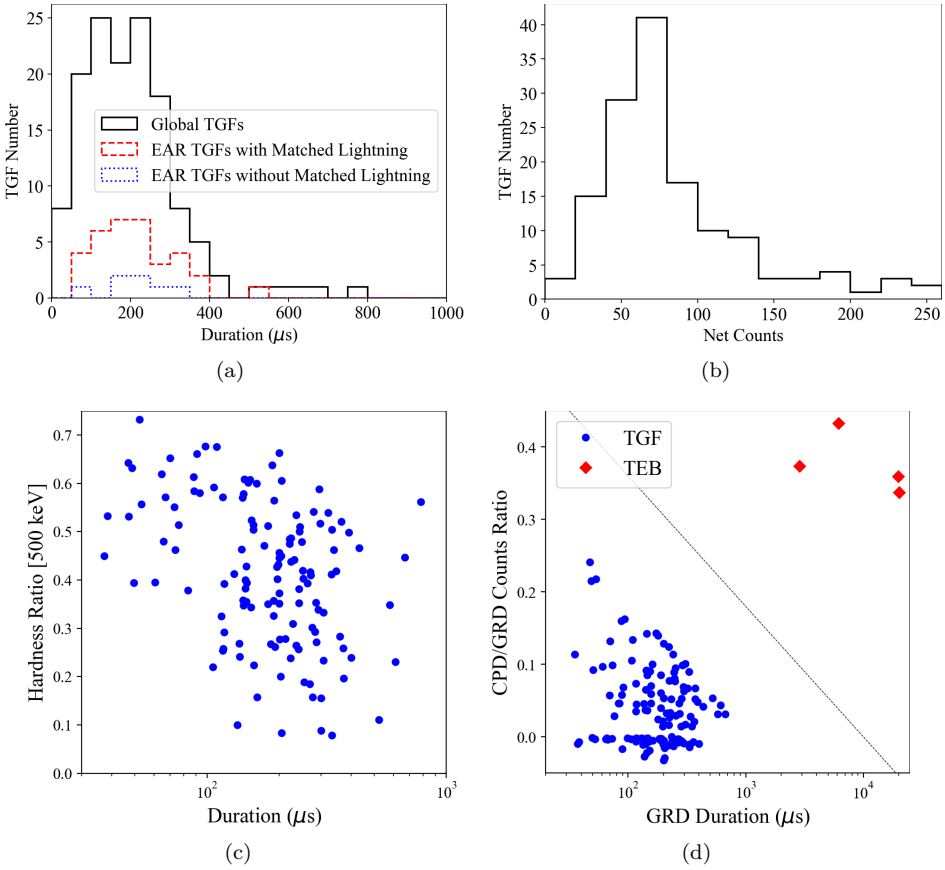

Figure 3. Statistical properties of GECAM TGFs and TEBs. (a) The duration distribution of TGFs. The duration is calculated by the Bayesian Blocks algorithm. The black, red, and blue lines illustrate the duration distribution of total TGFs (147), TGFs with (34), and without (8) associated GLD360 lightning in the EAR, respectively. (b) The distribution of the observed net counts for total TGFs. (c) The scatter plot of the duration of TGF events versus hardness ratio (energy limitation 500 keV). (d) The scatter plot of duration versus CPD/GRD counts ratio for TGFs and TEBs. The dashed line shows a tentative threshold of equation $y = -0.18 \times \log_{10}(x) + 0.72$ for TGF/TEB classification, where x is the duration (μs) and y is the CPD/GRD counts ratio.

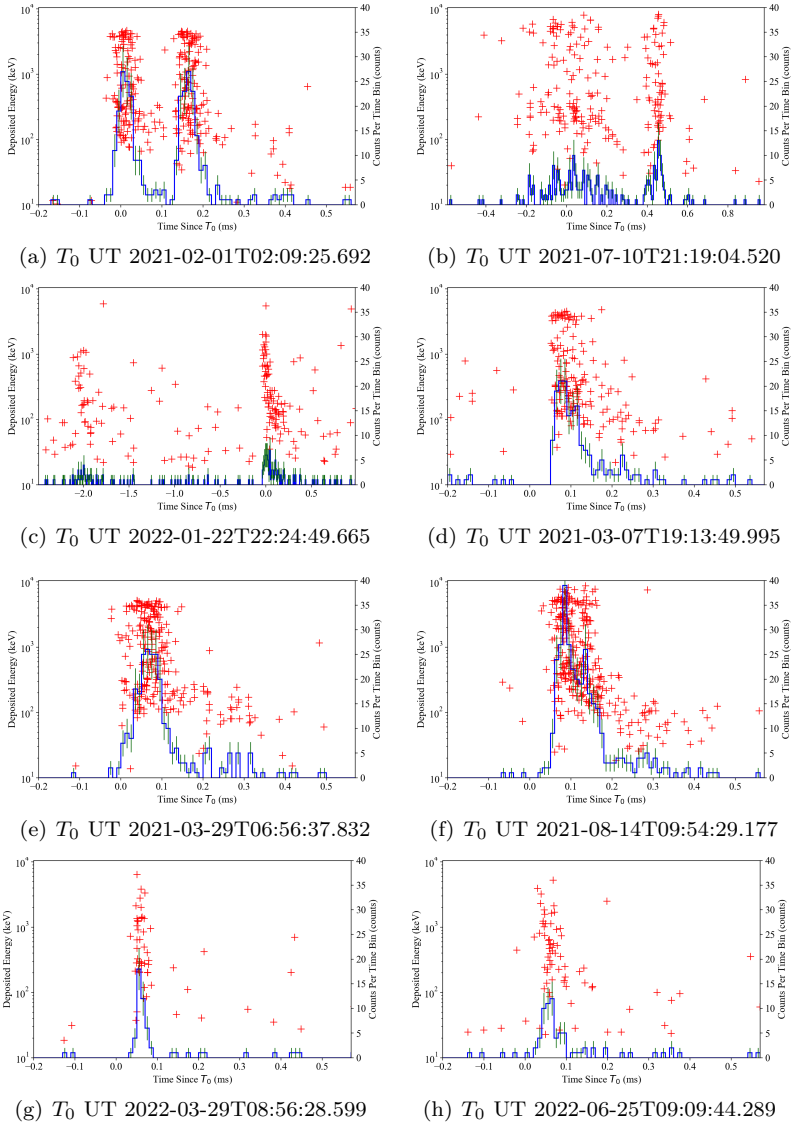

(a) T_0 UT 2021-02-01T02:09:25.692

(b) T_0 UT 2021-07-10T21:19:04.520

(c) T_0 UT 2022-01-22T22:24:49.665

(d) T_0 UT 2021-03-07T19:13:49.995

(e) T_0 UT 2021-03-29T06:56:37.832

(f) T_0 UT 2021-08-14T09:54:29.177

(g) T_0 UT 2022-03-29T08:56:28.599

(h) T_0 UT 2022-06-25T09:09:44.289

Figure 4. The light curves and time-energy scatters of characteristic GECAM TGFs. (a) to (c): multipeak TGFs. (d) to (f): bright TGFs with > 150 counts in duration. Note the overlapping pulse of (f). (g) to (h): short-duration TGFs (37 μs and 65 μs). The black histograms and red crosses show the light curves and time-energy scatters, respectively. The vertical and horizontal for all TGFs are on the same scales except for (b) and (c).

4 GECAM TEBs

The GECAM CPDs are mostly used to detect electrons and positrons in orbit, while it has low detection efficiency to gamma-ray (Xu et al., 2022). To distinguish between TGFs and TEBs, we find a very effective threshold considering the duration and CPD/GRD counts ratio (see Figure 3d).

In this paper, we present four high-confidence TEBs, as shown in Figure 2, Figure 3d, and Figure 5. Although TEBs can also produce many counts in GRDs, their duration and the CPD/GRD counts ratio is remarkably different from TGFs. It is explicitly shown in Figure 3d that the TEBs and TGFs are separated into two groups according to duration and CPD/GRD counts ratio. The CPD/GRD counts ratio for all TGFs is < 0.25 and mostly < 0.15, while that of TEBs reaches ~ 0.35. It should be noticed that the negative values of the CPD/GRD counts ratio mean no significant signals registered in CPDs. The duration of TGFs (< 1 ms) and TEBs (> 2 ms) are also distinctively different.

GECAM-B detected an interesting TEB event with two pulses separated by ~ 150 ms (Figure 5a) that occurred over the Southwest Indian Ocean at 18:34:40.552 UTC on September 11th, 2021. Unlike the bright main peak and weak return peak in a typical TEB, these two pulses have similar brightness. Since TEB electrons will travel along the Earth's magnetic field lines, we trace this line using the International Geomagnetic Reference Field (IGRF) 13 model (Alken et al., 2021). As shown in Figure 5e and 5f, there is no lightning activity around the GECAM nadir (51.2° E, 28.9° S, 587.7 km) and the southern magnetic footpoint (-31.3° E, 52.8° N, 40 km) within ± 1 minute of the TEB time and a radius of 1200 km. However, there is a cluster of WWLLN lightning around the northern magnetic footpoint (44.1° E, 45.5° N, 40 km) within 400 km and ± 10 seconds. Moreover, the expected round-trip bounce time between the GECAM-B satellite and the southern footpoint is $<\sim 17$ ms for 100 keV electrons, which is an order of magnitude lower than the observed time interval between the two pulses, strongly disfavoring the return peak nature of the second pulse.

Considering the lack of lightning discharge in the southern part and intense lightning activity in the northern part, as well as the expected time interval for TEB electrons, bounce from GECAM and the southern footpoint is far less than 150 ms, it is highly likely that the TEB electrons of both pulses originate from TGFs occurred around the northern footpoint in the same lightning discharge process. Even if they are produced by two TGF events, the distance between these two TGFs should not be very far, otherwise, they would not be detected as TEB at the same location of GECAM-B. As far as we are aware of, this TEB is the first reported event with two pulses that originate from the same geomagnetic footpoint.

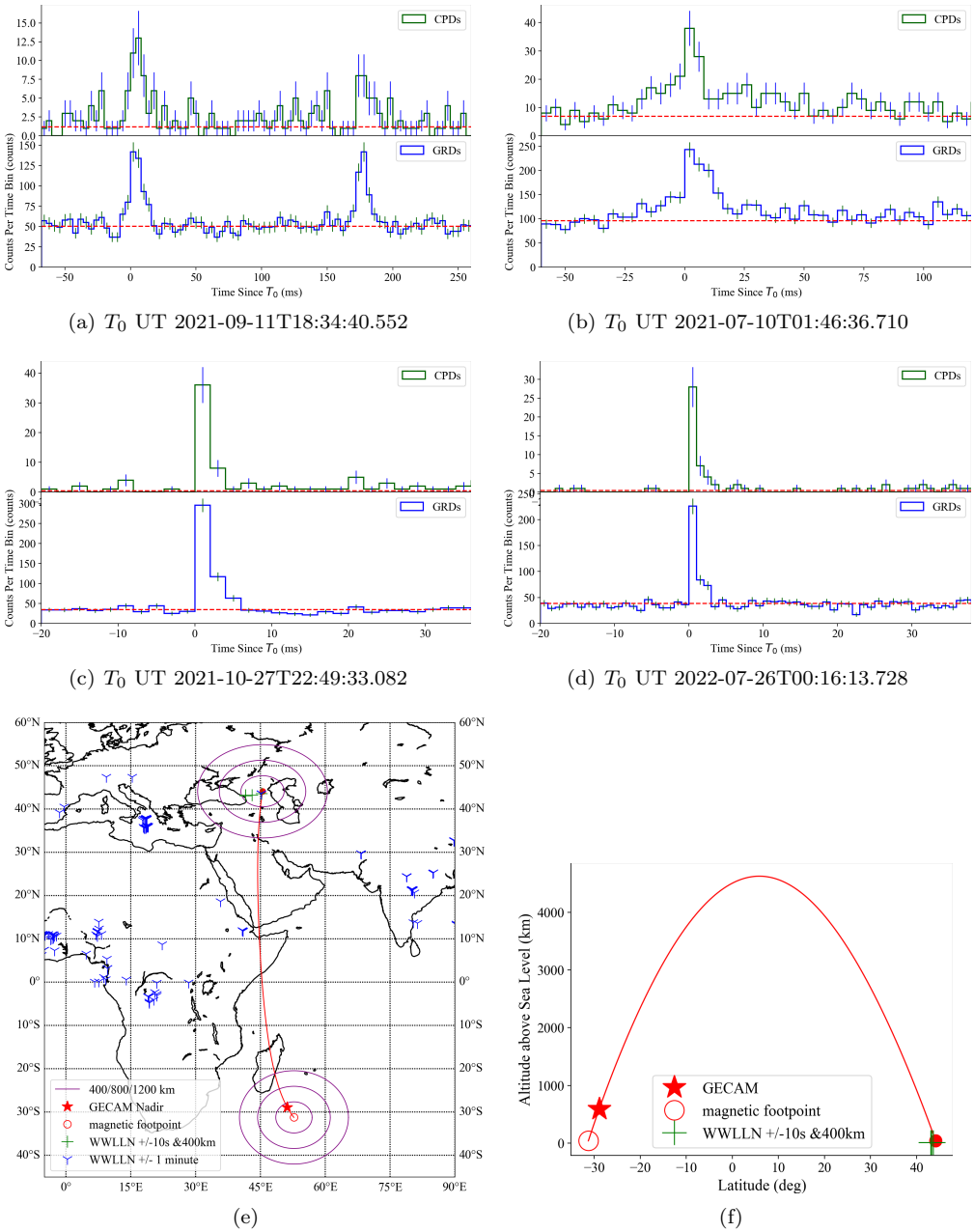

(a) T_0 UT 2021-09-11T18:34:40.552

(b) T_0 UT 2021-07-10T01:46:36.710

(c) T_0 UT 2021-10-27T22:49:33.082

(d) T_0 UT 2022-07-26T00:16:13.728

(e)

(f)

Figure 5. (a) to (d) The light curves of 4 GECAM TEBs. For each TEB, the upper and lower panels show the light curves of CPDs and GRDs, respectively. It should be noted that there are two pulses which episode by $\sim$ 150 ms on subfigure (a). (e) Map of GECAM nadir (red star), WWLLN lightning (blue triangles and green pluses), the traced magnetic field line (red line), and their footpoints (red circles) for the TEBs shown in subfigure (a). (f) The latitude-altitude projected map of the TEBs shown in subfigure (a). The blue triangles illustrate total WWLLN detections within 60 seconds, and green pluses illustrate the WWLLN lightning around the northern magnetic footpoint 400 km within 10 seconds. The solid red circle shows the northern magnetic footpoint and the hollow red circle shows the southern magnetic footpoint.

5 Conclusion

With novel designs on detectors and electronics, GECAM is a new powerful instrument to detect and identify TGFs and TEBs, as well as study their properties. Thanks to the high time resolution (100 ns), broad detection energy range (several keV to several MeV), and anti-saturation designs, GECAM can record very bright TGFs and TEBs, and reveal their fine structures in light curves and spectrum, which can help us better understand the production mechanism of TGFs and TEBs.

In this paper, a GECAM TGF/TEB search algorithm is proposed, then 147 bright TGFs and 4 TEBs are identified. The TGF detection rate for GECAM-B is $\sim$ 200 TGFs/year, which will increase if we loose the search threshold. The GECAM-GLD360 lightning-association ratio reaches $\sim$ 80% in the east Asia region, significantly higher than previous results obtained with the other space-borne instruments and the WWLLN data. A few interesting structures of TGFs are notable, such as a short spike (down to $\sim$ 10 μs) lying on the decay phase of the main pulse, an interesting double-peak TGF with very similar temporal and spectral distribution, and more than 40 counts are registered in an extremely short duration of $\sim$ 37 μs.

For mostly gamma-ray space telescopes, determining a TEB is not straightforward, e.g. through the 511 keV line of the spectrum and the return peak. With the joint observation of GRDs and CPDs, GECAM can directly distinguish between TGFs and TEBs according to the duration distribution and CPD/GRD counts ratio. We find an interesting TEB with two pulses which probably originated from a special lightning discharge process.

Acknowledgments

The GECAM (HuaiRou-1) mission is supported by the Strategic Priority Research Program on Space Science of the Chinese Academy of Sciences, China. This work is supported by the National Key R&D Program of China (2021YFA0718500). We thank the support from the Strategic Priority Research Program on Space Science, the Chinese Academy of Sciences (Grant No. XDA15360102, XDA15360300, XDA15052700), the National Natural Science Foundation of China (Grant No. 12273042, 12173038, 42274205, U1938115, U2038106), the National HEP Data Center (Grant No. E029S2S1) and the open fund of Hubei Luojia Laboratory (Grant No. 220100051). We thank Xi Long (Harvard University) for the helpful discussions. The GLD360 data used in this paper belong to Vaisala Inc who supports the ASIM project. The authors wish to thank the World Wide Lightning Location Network (http://wwlln.net) as a collaboration of more than 50 universities.

References

Alken, P., Thébault, E., Beggan, C. D., Amit, H., Aubert, J., Baerenzung, J., … others (2021). International geomagnetic reference field: the thirteenth generation. *Earth, Planets and Space*, *73*(1), 1–25.

An, Z. H., Sun, X. L., Zhang, D. L., Yang, S., Li, X. Q., Wen, X. Y., … Zhou, X. (2022). The design and performance of grd onboard the gecam satellite [Journal Article]. *Radiation Detection Technology and Methods*, *6*(1), 43-52. Retrieved from `https://doi.org/10.1007/s41605-021-00289-y` doi: 10.1007/s41605-021-00289-y

Briggs, M. S., Fishman, G., Connaughton, V., Bhat, P., Paciesas, W., Preece, R., … others (2010). First results on terrestrial gamma ray flashes from the fermi gamma-ray burst monitor. *Journal of Geophysical Research: Space Physics*, *115*(A7).

Briggs, M. S., Xiong, S., Connaughton, V., Tierney, D., Fitzpatrick, G., Foley, S., … others (2013). Terrestrial gamma-ray flashes in the fermi era: Improved observations and analysis methods. *Journal of Geophysical Research: Space Physics*, *118*(6), 3805–3830.

Cai, C., Xiong, S. L., Li, C. K., Liu, C. Z., Zhang, S. N., Li, X. B., … Zhou, D. K. (2021, 09). Search for gamma-ray bursts and gravitational wave electromagnetic counterparts with High Energy X-ray Telescope of Insight-HXMT. *Monthly Notices of the Royal Astronomical Society*, *508*(3), 3910-3920. Retrieved from `https://doi.org/10.1093/mnras/stab2760` doi: 10.1093/mnras/stab2760

Cai, C., Xiong, S.-L., Xue, W.-C., Zhao, Y., Xiao, S., Yi, Q.-B., … Zhang, F. (2022, 10). Burst search method based on likelihood ratio in Poisson statistics. *Monthly Notices of the Royal Astronomical Society*, *518*(2), 2005-2014. Retrieved from `https://doi.org/10.1093/mnras/stac3075` doi: 10.1093/mnras/stac3075

Celestin, S., & Pasko, V. P. (2011). Energy and fluxes of thermal runaway electrons produced by exponential growth of streamers during the stepping of lightning leaders and in transient luminous events. *Journal of Geophysical Research: Space Physics*, *116*(A3).

Celestin, S., Xu, W., & Pasko, V. (2013). Spectra of x-ray and gamma-ray bursts produced by stepping lightning leaders. In *Egu general assembly conference abstracts* (p. 13065).

Chanrion, O., & Neubert, T. (2010). Production of runaway electrons by negative streamer discharges. *Journal of Geophysical Research: Space Physics*, *115*(A6).

Dwyer, J. (2003). A fundamental limit on electric fields in air. *Geophysical Research Letters*, *30*(20).

Dwyer, J. (2008). Source mechanisms of terrestrial gamma-ray flashes. *Journal of Geophysical Research: Atmospheres*, *113*(D10).

Dwyer, J. (2012). The relativistic feedback discharge model of terrestrial gamma ray flashes. *Journal of Geophysical Research: Space Physics*, *117*(A2).

Dwyer, J. R. (2010). Diffusion of relativistic runaway electrons and implications for lightning initiation. *Journal of Geophysical Research: Space Physics*, *115*(A3).

Dwyer, J. R., Grefenstette, B. W., & Smith, D. M. (2008). High-energy electron beams launched into space by thunderstorms. *Geophysical Research Letters*, *35*(2).

Dwyer, J. R., Schaal, M. M., Cramer, E., Arabshahi, S., Liu, N., Rassoul, H., … Uman, M. A. (2012). Observation of a gamma-ray flash at ground level in association with a cloud-to-ground lightning return stroke. *Journal of Geophysical Research: Space Physics*, *117*(A10).

Dwyer, J. R., & Smith, D. M. (2005). A comparison between monte carlo simulations of runaway breakdown and terrestrial gamma-ray flash observations.

Geophysical Research Letters, *32*(22).

Feng, H., Li, T., Wu, M., Zha, M., & Zhu, Q. (2002). Temporal and spectral properties of gamma-ray flashes. *Geophysical research letters*, *29*(3), 6–1.

Fishman, G. J., Bhat, P. N., Mallozzi, R., Horack, J. M., Koshut, T., Kouveliotou, C., … Christian, H. J. (1994). Discovery of intense gamma-ray flashes of atmospheric origin. *Science*, *264*(5163), 1313–1316. Retrieved 2022-05-05, from http://www.jstor.org/stable/2884079

Goldstein, A., Veres, P., Burns, E., Briggs, M. S., Hamburg, R., Kocevski, D., … Stanbro, M. (2017, oct). An ordinary short gamma-ray burst with extraordinary implications: Fermi-gbm detection of grb 170817a. *The Astrophysical Journal*, *848*(2), L14. Retrieved from https://doi.org/10.3847/2041-8213/aa8f41 doi: 10.3847/2041-8213/aa8f41

Grefenstette, B. W., Smith, D. M., Hazelton, B., & Lopez, L. (2009). First rhessi terrestrial gamma ray flash catalog. *Journal of Geophysical Research: Space Physics*, *114*(A2).

Gurevich, A., Milikh, G., & Roussel-Dupre, R. (1992). Runaway electron mechanism of air breakdown and preconditioning during a thunderstorm. *Physics Letters A*, *165*(5-6), 463–468.

Han, X., Zhang, K., Huang, J., YU, J., XIONG, S., CHEN, Y., … GENG, H. (2020). Gecam satellite system design and technological characteristic [Journal Article]. *SCIENTIA SINICA Physica, Mechanica & Astronomica*, *50*(1674-7275), 129507. Retrieved from https://www.sciengine.com/publisher/ScienceChinaPress/journal/SCIENTIASINICAPhysica,Mechanica\&Astronomica/50/12/10.1360/SSPMA-2020-0120 doi: https://doi.org/10.1360/SSPMA-2020-0120

Klebesadel, R. W., Strong, I. B., & Olson, R. A. (1973). Observations of gamma-ray bursts of cosmic origin. *The Astrophysical Journal*, *182*, L85.

Li, et al. (2022). The technology for detection of gamma-ray burst with GECAM satellite. *Radiation Detection Technology and Methods*. doi: 10.1007/s41605-021-00288-z

Lindanger, A., Marisaldi, M., Maiorana, C., Sarria, D., Albrechtsen, K., Østgaard, N., … others (2020). The 3rd agile terrestrial gamma ray flash catalog. part i: Association to lightning sferics. *Journal of Geophysical Research: Atmospheres*, *125*(11), e2019JD031985.

Liu, N., & Dwyer, J. R. (2013). Modeling terrestrial gamma ray flashes produced by relativistic feedback discharges. *Journal of Geophysical Research: Space Physics*, *118*(5), 2359–2376.

Liu, Y., Gong, K., Li, X., Wen, X., An, Z., Cai, C., … others (2021). The sipm array data acquisition algorithm applied to the gecam satellite payload. *arXiv preprint arXiv:2112.04786*.

Lorimer, D. R., Bailes, M., McLaughlin, M. A., Narkevic, D. J., & Crawford, F. (2007). A bright millisecond radio burst of extragalactic origin. *Science*, *318*(5851), 777–780.

Lu, G., Blakeslee, R. J., Li, J., Smith, D. M., Shao, X.-M., McCaul, E. W., … Cummer, S. A. (2010). Lightning mapping observation of a terrestrial gamma-ray flash. *Geophysical Research Letters*, *37*(11).

Lu, G., Cummer, S. A., Li, J., Han, F., Smith, D. M., & Grefenstette, B. W. (2011). Characteristics of broadband lightning emissions associated with terrestrial gamma ray flashes. *Journal of Geophysical Research: Space Physics*, *116*(A3).

Lyu, F., Cummer, S. A., Lu, G., Zhou, X., & Weinert, J. (2016). Imaging lightning intracloud initial stepped leaders by low-frequency interferometric lightning mapping array. *Geophysical Research Letters*, *43*(10), 5516–5523.

Maiorana, C., Marisaldi, M., Lindanger, A., Østgaard, N., Ursi, A., Sarria, D., … others (2020). The 3rd agile terrestrial gamma-ray flashes catalog. part ii: Optimized selection criteria and characteristics of the new sample. *Journal of*

Geophysical Research: Atmospheres, *125*(11), e2019JD031986.

Marisaldi, M., Fuschino, F., Labanti, C., Galli, M., Longo, F., Del Monte, E., … others (2010). Detection of terrestrial gamma ray flashes up to 40 mev by the agile satellite. *Journal of Geophysical Research: Space Physics*, *115*(A3).

Marisaldi, M., Galli, M., Labanti, C., Østgaard, N., Sarria, D., Cummer, S., … others (2019). On the high-energy spectral component and fine time structure of terrestrial gamma ray flashes. *Journal of Geophysical Research: Atmospheres*, *124*(14), 7484–7497.

Mezentsev, A., Østgaard, N., Gjesteland, T., Albrechtsen, K., Lehtinen, N., Marisaldi, M., … Cummer, S. (2016). Radio emissions from double rhessi tgfs. *Journal of Geophysical Research: Atmospheres*, *121*(13), 8006–8022.

Moss, G. D., Pasko, V. P., Liu, N., & Veronis, G. (2006). Monte carlo model for analysis of thermal runaway electrons in streamer tips in transient luminous events and streamer zones of lightning leaders. *Journal of Geophysical Research: Space Physics*, *111*(A2).

Nemiroff, R. J., Bonnell, J. T., & Norris, J. P. (1997). Temporal and spectral characteristics of terrestrial gamma flashes. *Journal of Geophysical Research: Space Physics*, *102*(A5), 9659–9665.

Østgaard, N., Neubert, T., Reglero, V., Ullaland, K., Yang, S., Genov, G., … others (2019). First 10 months of tgf observations by asim. *Journal of Geophysical Research: Atmospheres*, *124*(24), 14024–14036.

Poelman, D. R., Schulz, W., & Vergeiner, C. (2013). Performance characteristics of distinct lightning detection networks covering belgium. *Journal of Atmospheric and Oceanic Technology*, *30*(5), 942–951.

Pohjola, H., & Mäkelä, A. (2013). The comparison of gld360 and euclid lightning location systems in europe. *Atmospheric research*, *123*, 117–128.

Roberts, O. J., Fitzpatrick, G., Stanbro, M., McBreen, S., Briggs, M. S., Holzworth, R. H., … Mailyan, B. G. (2018). The first fermi-gbm terrestrial gamma ray flash catalog. *Journal of Geophysical Research: Space Physics*, *123*(5), 4381-4401. Retrieved from `https://agupubs.onlinelibrary.wiley.com/doi/abs/10.1029/2017JA024837` doi: https://doi.org/10.1029/2017JA024837

Said, R., Cohen, M., & Inan, U. (2013). Highly intense lightning over the oceans: Estimated peak currents from global gld360 observations. *Journal of Geophysical Research: Atmospheres*, *118*(13), 6905–6915.

Sarria, D., Østgaard, N., Kochkin, P., Lehtinen, N., Mezentsev, A., Marisaldi, M., … others (2021). Constraining spectral models of a terrestrial gamma-ray flash from a terrestrial electron beam observation by the atmosphere-space interactions monitor. *Geophysical Research Letters*, *48*(9), e2021GL093152.

Scargle, J. D., Norris, J. P., Jackson, B., & Chiang, J. (2013, feb). Studies in astronomical time series analysis. vi. bayesian block representations. *The Astrophysical Journal*, *764*(2), 167. Retrieved from `https://doi.org/10.1088/0004-637x/764/2/167` doi: 10.1088/0004-637x/764/2/167

Skeltved, A. B., Østgaard, N., Mezentsev, A., Lehtinen, N., & Carlson, B. (2017). Constraints to do realistic modeling of the electric field ahead of the tip of a lightning leader. *Journal of Geophysical Research: Atmospheres*, *122*(15), 8120–8134.

Stolzenburg, M., Marshall, T. C., Karunarathne, S., & Orville, R. E. (2016). Luminosity with intracloud-type lightning initial breakdown pulses and terrestrial gamma-ray flash candidates. *Journal of Geophysical Research: Atmospheres*, *121*(18), 10–919.

Ursi, A., Guidorzi, C., Marisaldi, M., Sarria, D., & Frontera, F. (2017). Terrestrial gamma-ray flashes in the bepposax data archive. *Journal of Atmospheric and Solar-Terrestrial Physics*, *156*, 50–56.

Wilson, C. T. (1925). The acceleration of β-particles in strong electric fields such as those of thunderclouds. In *Mathematical proceedings of the cambridge philo-*

sophical society (Vol. 22, pp. 534–538).

Woods, P., & Thompson, C. (2004). Soft gamma repeaters and anomalous x-ray pulsars: magnetar candidates. *arXiv preprint astro-ph/0406133*.

Xiao, S., Liu, Y., Peng, W., An, Z., Xiong, S., Tuo, Y., … others (2022). On-ground and on-orbit time calibrations of gecam. *Monthly Notices of the Royal Astronomical Society*, *511*(1), 964–971.

Xiong, S., Briggs, M., Connaughton, V., Fishman, G., Tierney, D., Fitzpatrick, G., … Hutchins, M. (2012). Location prediction of electron tgfs. *Journal of Geophysical Research: Space Physics*, *117*(A2).

Xu, W., Celestin, S., & Pasko, V. P. (2012). Source altitudes of terrestrial gamma-ray flashes produced by lightning leaders. *Geophysical Research Letters*, *39*(8).

Xu, W., Celestin, S., & Pasko, V. P. (2015). Optical emissions associated with terrestrial gamma ray flashes. *Journal of Geophysical Research: Space Physics*, *120*(2), 1355–1370.

Xu, Y. B., Li, X. Q., Sun, X. L., Yang, S., Wang, H., Peng, W. X., … Zhou, X. (2022). The design and performance of charged particle detector onboard the gecam mission [Journal Article]. *Radiation Detection Technology and Methods*, *6*(1), 53-62. Retrieved from `https://doi.org/10.1007/s41605-021-00298-x` doi: 10.1007/s41605-021-00298-x

Zhang, et al. (2022). Dedicated sipm array for grd of gecam. *Radiation Detection Technology and Methods*, *6*(1), 63–69.

Zhao, X., Xiong, S., Wen, X., Li, X., Cai, C., Xiao, S., & Luo, Q. (2021, December). The In-Flight Realtime Trigger and Localization Software of GECAM. *arXiv e-prints*, arXiv:2112.05101.

Zhao, Y., Xue, W., Xiong, S., Luo, Q., YQ, Z., H, Y., … SN, Z. (2022, September). On the Localization Methods of High Energy Transients for All-Sky Gamma-Ray Monitors. *arXiv e-prints*, arXiv:2209.13088.

Zhao, Y., Xue, W., Xiong, S., Wang, Y., Liu, J., Luo, Q., … Yu, H. (2022, November). GECAM Localization of High Energy Transients and the Systematic Error. *arXiv e-prints*, arXiv:2211.15570.